applications, IEEE Trans Microwave Theory Tech 52 (2004), 1479–1489.
5. L. DiDomenico and G. Rebeiz, Digital communications using self-phased arrays, IEEE Trans Microwave Theory Tech 49 (2001), 677–684.

STABILITY ANALYSIS IN A SOLITON FIBER RING LASER WITH A HYBRID SATURABLE ABSORBER

M. R. A. Moghaddam,[1] S. W. Harun,[1,2] K. S. Lim,[1] and H. Ahmad[1]
[1] Photonics Research Center, University of Malaya, Kuala Lumpur 50603, Malaysia; Corresponding author: mramoghaddam@gmail.com
[2] Department of Electrical Engineering, University of Malaya, 50603 Kuala Lumpur, Malaysia

Received 18 April 2012

ABSTRACT: *A stable mode-locked fiber laser having two rejection ports employing a 4 m long erbium doped fiber is demonstrated. Near transform limited short pulses with a repetition rate of 8.27 MHz are obtained at a wavelength of 1565 nm by using a slow saturable absorber. The pulse width can continuously vary from 1.2 ps to less than 130 fs with a maximum spectral width of 20 nm. Although the changes of the pulse duration over one round-trip in the resonator is small. However, a comparison of the energy fluctuations from coupler port toward polarizing beam splitter (PBS) port reveals that energy fluctuation is varied from 4.1% to 7.8% and stronger for PBS port. We also find that the low frequency timing jitter for a fixed pump power is stronger for PBS port and the high frequency timing jitter at PBS port is more than twice larger than that of the timing jitter at coupler port. By removing fiber adapters and controlling the environmental airflow in the setup, timing jitter was reduced by an order of magnitude.* © 2012 Wiley Periodicals, Inc. Microwave Opt Technol Lett 55:164–170, 2013; View this article online at wileyonlinelibrary.com. DOI 10.1002/mop.27220

Key words: *erbium; fiber laser; mode-locking; slow saturable absorber*

1. INTRODUCTION

Generation of mode locked laser in fiber offers many advantages such as, having compact sizes, being maintenance- and alignment-free, possessing superior thermal handling, inherent stability and immunity against thermo-optical issues. An all-fiber, unidirectional mode locked ring laser was implemented by Tamura et al. [1]. At the same time, the use of semiconductor saturable absorber mirrors (SESAMs) as a pulse shaping element made a breakthrough in passive mode locked fiber laser with self starting and stable operation modes [2]. This type of laser is being used in medical applications [3], telecommunication [4, 5], and micromachining applications [6].

Several different physical mechanisms can be used for passive mode-locking. Additive pulse mode-locking (P-AMP) and the nonlinear amplifying loop mirror (NALM) techniques applied in passive mode locking rely on the Kerr effect in the length of optical fiber in conjunction with polarizers to introduce artificial saturable absorber (SA) action [7]. Hence passive mode locking can be achieved by exploiting the changes in intensity dependent state of polarization which is caused by SPM and XPM in cavity. In a ring cavity structure, a polarizing isolator and one or two polarization controllers act as artificial SA [8]. P-AMP exhibits extremely fast absorption behavior with wide tunability and no practical limitations on pulse duration or wavelength of operation. However, this method suffers from gradual polarization drift, time-varying linear and nonlinear phase delays among eigenmodes of the fiber and finally degradation of mode locked pulse due to effect of temperature drift and mechanical stress on fiber sections. Furthermore, such approach demands regular adjustment of the structure to operate in the optimum condition and to compensate any degradation of pulse quality. On the other hand, NALM shows the tendency for operation with bursts of multiple pulses because of long cavity lengths [9].

As a third method, SA layers were introduced in optical devices to examine their nonlinear optical property of an intensity-dependent absorption for ultrafast all-optical switching [10]. In a slow SA there is a temporal range with net gain just after the pulses. In general, an anti-resonant SA for transmission applications can lead to a high-repetition-rate cavity with fewer required components and without significant dispersion influence of SA. In this work, P-AMP techniques besides using SA have been used to enhance pulse shortening.

2. INFLUENCE OF DISPERSION ON MODE LOCKING REGIME

The pulse characteristics and its formation in cavity strongly depend on net-dispersion of cavity. Clearly dispersion will cause the pulse to broaden. The nonlinear mode-locking mechanism to some extent balances this broadening tendency, though minimizing linear dispersion is still necessary [11]. In general, for zero SPM the minimum pulsewidth occurs at zero GVD. As SPM increases, the point of minimum pulsewidth moves to negative GVD where the chirp is compensated. As a final remark proper balance of GVD and SPM reduces the pulse duration by a factor of 2.75 [8]. It is also possible to distinguish three stable operation regimes, depending on the dominant pulse shaping mechanisms: (i) soliton pulse regime determined by the balance between anomalous dispersion and self-phase modulation, (ii) stretched-pulse regime determined by dispersion-managed solitons, and (iii) self-similar pulse regime determined by the interrelation of normal dispersion and finite-bandwidth gain.

3. SOLITON PULSE REGIME

It has been proven that SPM alone in the positive dispersion regime should always be kept small. A rule of thumb is that the nonlinear phase shift for the peak should be at most a few mrad per 1% of modulation depth. In fact in the sub-picosecond domain, SPM could hardly be made weak enough. Hence, soliton regime is commonly needed in this domain. In a simple scheme of having a SA, especially in the picosecond domain, a large modulation depth supports shorter pulses, but there is an upper limit for modulation depth (ΔR) of SA due to the stability limit. To have a stable picosecond pulse train, the critical intracavity pulse energy $E_{p,c}$ is recommended to be as $E_p^2 > E_{p,c}^2 = E_L^{sat} E_A^{sat} \Delta R$ [7] where E_p is the intracavity pulse energy, E_L^{sat} is the saturation energy of the gain medium, E_A^{sat} is the saturation energy of the SA. Indeed, soliton pulses with duration up to about a factor of 40 times shorter than the absorber recovery time have been demonstrated. Even with SA, SPM can make the system unstable unless sufficient dispersion is introduced at the same time. The Haus's master differential equation can be solved analytically using soliton perturbation theory. The soliton pulse duration (FWHM) is given by τ_p and for a given negative dispersion (D) and an intracavity pulse energy (E_p), the shortest pulse duration is achieved by the net cavity GVD small and anomalous [12]. Based on the phase shift of the soliton per

TABLE 1 Specification of Fibers and SA for the Experimental Setups

Parameters	Value
SA (Batop, Germany)	Antiresonant
Modulation depth of SA	15%
Relaxation time of SA	2 ps
Non-saturable loss of SA	10%
Saturation fluence of SA	300 μj/cm^2
Absorbance of SA	25%
Dispersion—Antiresonant SA	No influence
EDFA (DF1500L)	3 m
Mode field diameter(MFD)	5.9 μm
Erbium absorption (975 nm)	12 dB/m
Erbium absorption cross section (σ_{ab})	(975 nm)
Dispersion GVD	23.51 ± 0.21 ps^2/km
Background loss, signal	40 dB/km
Dispersion—Corning SMF28 (1545 nm)	−22.75 ± 0.91 ps^2/km
Dispersion WDM (1548 nm)	−9.94 ± 0.18 ps^2/km

cavity round trip $\Phi_s = \delta_L P_0$ and the peak power (P_0) inside the laser cavity, the minimum pulse duration τ_p^{min} can be predicted as:

$$\tau_p^{min} \approx 0.45\left(\frac{1}{\Delta\nu_g}\right)^{\frac{3}{4}}\left(\frac{\tau_A}{\Delta R}\right)^{\frac{1}{4}}\frac{g^{\frac{3}{5}}}{\Phi^{\frac{1}{5}}}$$

It is important not only to adjust the ratio of dispersion and SPM to obtain the desired soliton pulse duration, but also to keep their absolute values in a reasonable range where the nonlinear phase change is in the order of some tens to a few hundred mrad per round trip [12].

Too small amounts of the nonlinear phase shift result in a stronger pulse shaping details of the SA. On the other hand, excessively strong nonlinear phase shifts per round trip can make Kelly sidebands [8] in the spectrum and make the pulses unstable. Generally this effect is a signature of soliton pulse losses. Consequently, the stability of the circulating solitons requires a very strong SA for femtosecond regime.

4. EXPERIMENTAL SETUP

The cavity consists a piece of Erbium doped fiber, a wavelength division multiplexing (WDM) coupler, a set of wave-plates, a polarizing beam splitter integrated with isolator (PBS-ISO), a SA, an isolator, a polarization controller (PC), and an output coupler (90/10). The SA specifications and typical fiber parameters are listed in Table 1. The laser oscillator consists of three different fibers namely a piece of 4 m long erbium doped fiber, a 0.42 m long WDM fiber, and for other sections of the ring cavity a piece of corning single mode fiber (SMF). The SMF fiber section between the gain media and the SA is fixed to approximately 1.9 m in all configurations.

Two output ports are utilized to measure and compare the pulse characteristics. These investigations are necessary for choosing the optimal resonator output positions for the different applications. Unidirectional operation is achieved by using PBS-ISO as a 50% rejection port. As shown in Figure 1, an oscilloscope combined with an autocorrelator (Femtochrome FR103XL), and a digital oscilloscope together with a photodetector are used to simultaneously monitor the pulse characteristics. For quantitative measurements of the noise, the signal from photodiode is analyzed through radio frequency spectrum analyzer (RFSA). The optical spectrum with a resolution of 0.07 nm is measured with an optical spectrum analyzer.

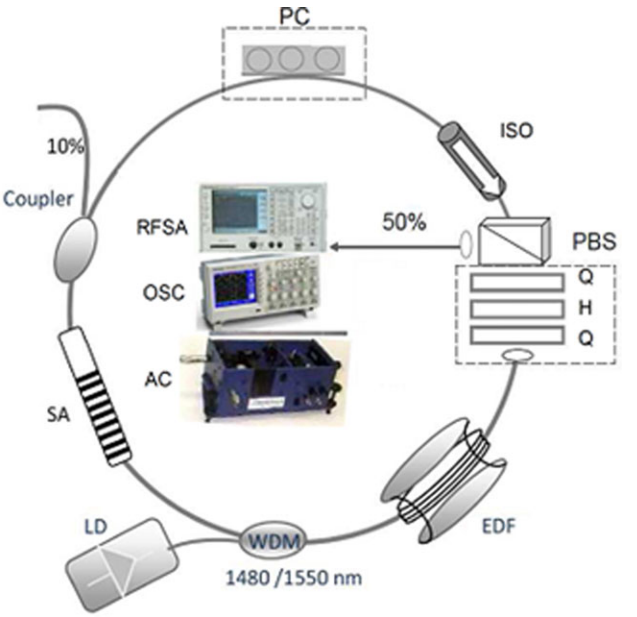

Figure 1 Experimental setup of the laser EDFL. "WDM: wavelength division multiplexer; SA: saturable absorber; OSC: oscilloscope; RFSA: RF spectrum analyzer; OSA: optical spectrum analyzer; AC: auto-correlator; PC: polarization controller; PBS-isolator: polarizing beam splitter integrated with isolator; *H*: (zero order)1/2-wave retarder; *Q*: (zero order) 1/4-wave retarder; ISO: isolator." [Color figure can be viewed in the online issue, which is available at wileyonlinelibrary.com]

5. EXPERIMENTAL RESULTS FOR MODE-LOCKED EDF LASER

At first the net cavity GVD in the proposed laser was set approximately to −0.04 ps^2, when the length of DF1500L was 4 m. In fact, the net GVD in the cavity for a given repetition rate (fixed cavity length) increases linearly by the length of DF1500L as shown in Figure 2.

Figure 3 compares the laser spectra, from the PBS output port and coupler port. The pump power is fixed at 100 mW in the figure. The polarization state along the spectrum is altered by polarization controllers. The spectrum changes from a narrow to a relatively broad one and the variation of the polarization state leads to a strong spectral filtering by the PBS. These

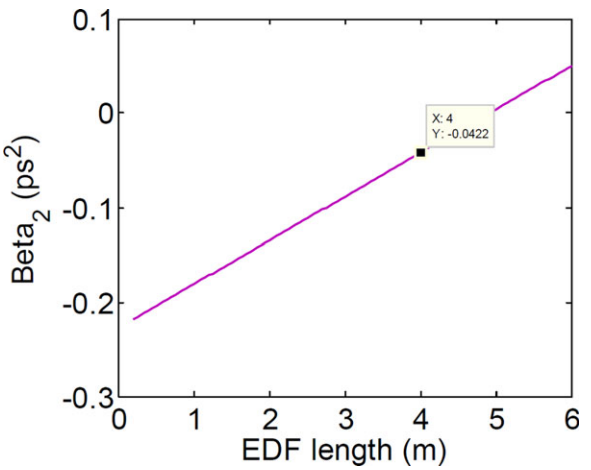

Figure 2 Net cavity dispersion for various lengths of EDF in the cavity. The total length of cavity is fixed at 10.4 m. [Color figure can be viewed in the online issue, which is available at wileyonlinelibrary.com]

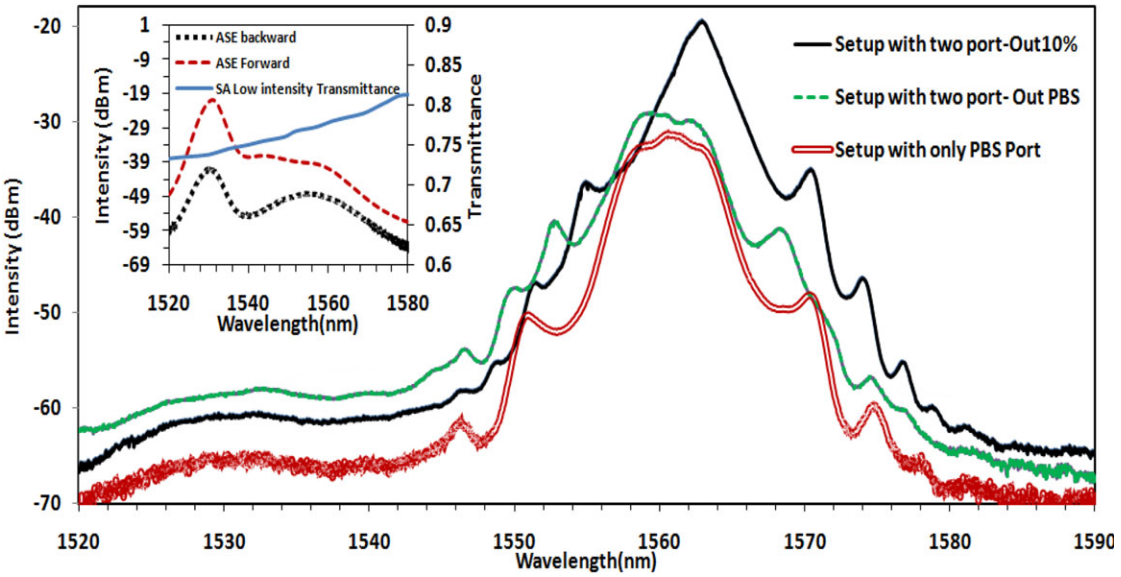

Figure 3 Spectra measured at different output ports for a ring cavity with 4 m long EDF (DF1500L). Pump power is fixed at 100 mW. Inset shows ASE spectra in forward and backward schemes and also transmittance spectrum (%) of SA. [Color figure can be viewed in the online issue, which is available at wileyonlinelibrary.com]

changes indicate transition from a CW to an initially Q-switching operation of the laser. Further adjustment results in broader spectrum and stable mode locked pulse train. As the output characteristics are extremely sensitive to the settings of the PCs, we might deduce that the nonlinear polarization rotation together with the PBS-ISO have crucial roles in the spectral and temporal filtering.

In this GVD map, optical bandwidth (FWHM) is observed to be approximately 5.64 nm with a resolution of 0.07 nm, implying 0.45 ps $Sech^2$-shaped transform-limited pulse duration. The spectrum shows indication of Kelly sidebands around the centre of the spectrum as they often arise in soliton lasers. The sidebands appeared as a pedestal under the pulse can contain an energy comparable to the pulse energy. It should be noted that the amount of continuum that is generated at a certain frequency is proportional to the spectral amplitude of the soliton at this frequency. As pulse width becomes shorter, sidebands would move closer to the center.

A log-scale AC trace shows that Kelly sidebands in optical spectrum correspond to a spreading pulse background or a very strong pedestal in the temporal profile. However, the existence of the pedestal does not affect the average duration.

Figure 4 depicts the measured intensity autocorrelation of this setup. Digital data are also fitted by MATLAB with a $sech^2$ profile. Inset of Figure 4, shows the pulse train from output coupler. As shown in the inset figure, the peak of ASE spectrum at 1530 nm is shifted to the peak of output spectra at 1560 nm due to the fact that the insertion loss and transmittance in EDF and SA naturally depend on the wavelength. The results show that for a given pump power, the spectral width increases by 10% and pulses get narrower at the PBS rejection port, when compared to that of the output coupler.

The mode-locking in this setup shows a SA dominated self-starting at a repetition rate of 9.87 MHz. An output power of 4.9 mW from the setup with a slope efficiency of about 5%, translate to pulse energies of 0.5 nJ, pulse durations of 1.2 ps,

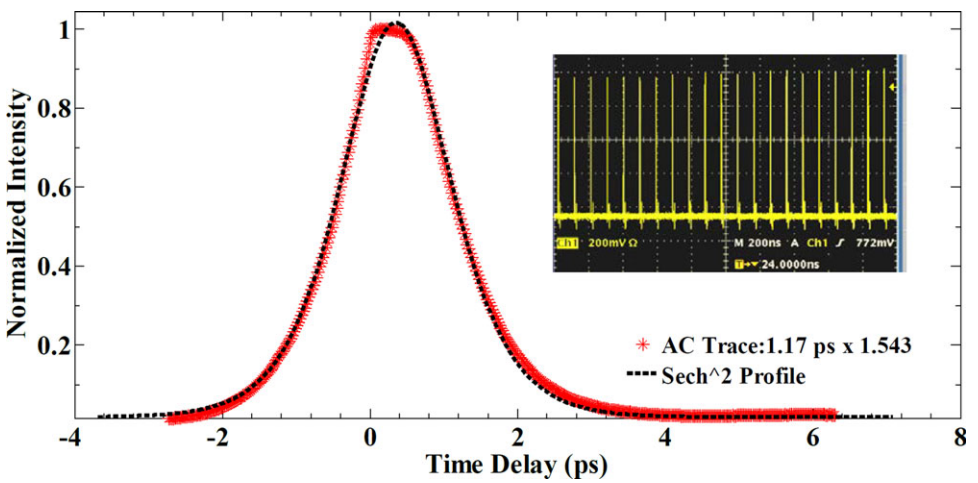

Figure 4 Autocorrelation trace and pulse train (inset) of the 1.17 ps pulses. Dashed curve: $sech^2$ fit. Inset pulse train of passive mode locked laser with repetition rate of 9.87 MHz. [Color figure can be viewed in the online issue, which is available at wileyonlinelibrary.com]

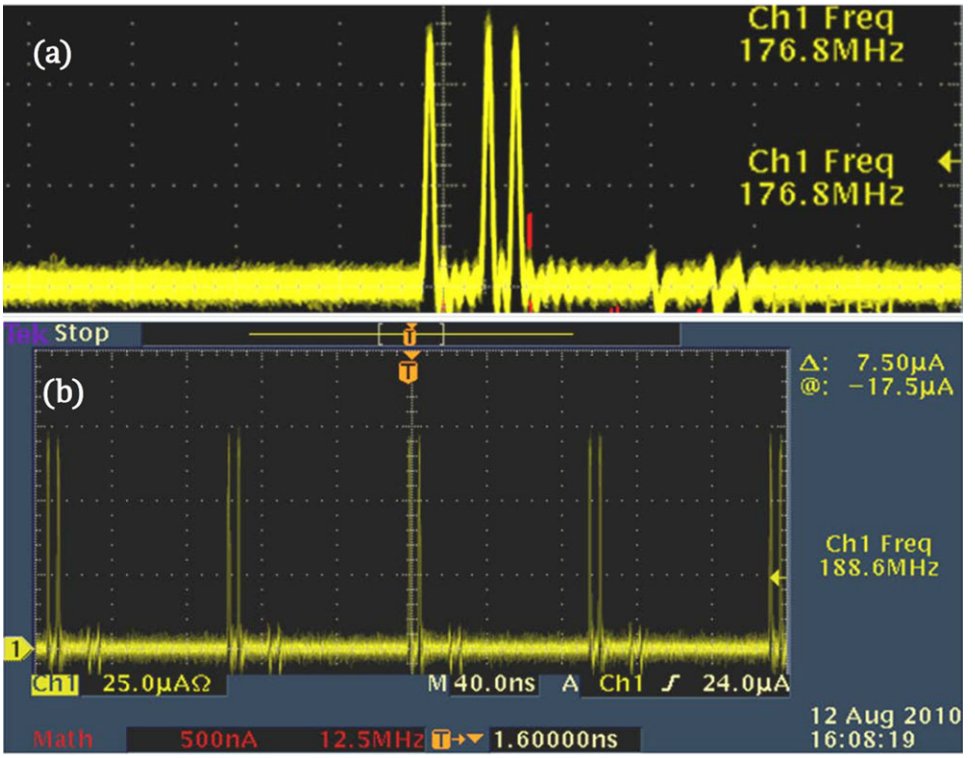

Figure 5 Period-doubling of multiple vector solitons: (a) Two vector solitons, (b) three vector solitons. [Color figure can be viewed in the online issue, which is available at wileyonlinelibrary.com]

and pulse peak powers of 0.42 kW. The time-bandwidth product was measured to be 0.81 for this setting.

The pump power threshold was measured to be 11 mW for laser oscillation while the measured threshold for mode-locking operation was 20 mW. By removing the 10% coupler, a more practical resonator is conducted with a higher repetition rate, lower ratio of the energy in the pedestals, lower resonator loss, and lower threshold for CW mode locking. The output spectrum of this configuration is also presented in Figure 3. The laser has almost similar characteristic compared to the laser configured with an output coupler. The difference is due to a shorter resonator length resulting in a higher repetition rate (13.75 MHz) with weaker nonlinear polarization rotation (NPR).

For comparison purposes, the experiments are repeated for a similar setup in the absence of SA, RC-PC, and PBS. In this configuration, the laser does not show self-starting mode-locking. The high repetition rate pulse train and the multiple pulses circulate within the cavity because of the phenomenon of soliton energy quantization. It is observed that without a polarizer in cavity, soliton circulation in the cavity exhibit complicate polarization dynamics. As shown in Figure 5, not only period-doubling of single vector soliton but also multiple vector solitons can be detected. By increasing the pump power, the number of vector solitons [13] circulating in the cavity is increased.

Employing the setup of Figure 1, the mode-locking again shows a self-starting which is SA dominated. Based on the nonlinear polarization evolution (NPE) in the SMF section and the spectral broadening in the EDF, the fiber section length between the SA and the PBS (2 m) is critical in the pulse shaping mechanism. The various lengths of SMF-28 in the cavity lead to changes in the sign and the value of net cavity GVD. Consequently, various types of pulses were observed at the PBS port

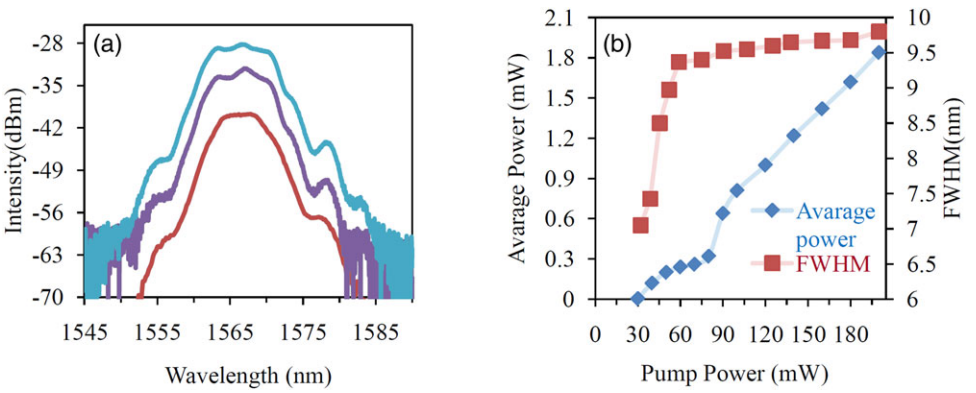

Figure 6 (a) Spectra measured at PBS port, (b) the variation of the spectral width, and output power as a function of the pump power at the PBS port. [Color figure can be viewed in the online issue, which is available at wileyonlinelibrary.com]

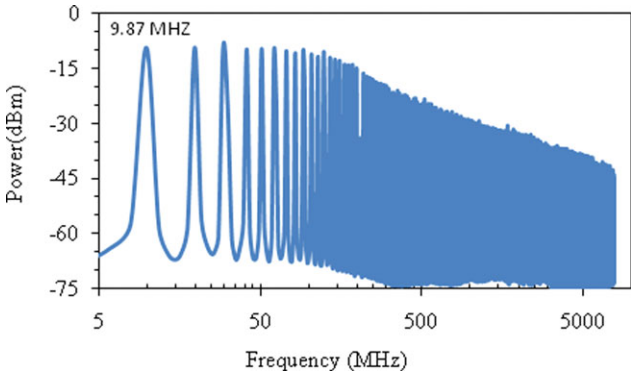

Figure 7 RF spectrum of pulse train for proposed oscillator without multiple pulsing. The frequency axis in this figure is logarithmic. [Color figure can be viewed in the online issue, which is available at wileyonlinelibrary.com]

such as stretched or parabolic pulses, fundamental soliton as well as the coexistence of a soliton with a tangible amount of continuum. By decreasing GVD to -0.30 ps^2, a noisy AC trace with strong coherence spikes was observed. This is a signature of leaving the regime of fundamental soliton generation.

It is possible to cut an adjusted length of SMF from setup to obtain a near zero GVD of the cavity. As illustrated in Figures 6(a) and 6(b), the effect of the sidebands can be avoided by decreasing the average dispersion of the cavity and the FWHM of the spectrum can be increased up to 9.8 nm. In this dispersion map, a higher pump power threshold of 40 mW is required for mode locking operation. From the figure, after putting an extra pump power, the output power is increased, but no further improvement of pulse duration and FWHM of the spectra are observed. The measured value of 9.8 nm for FWHM in the optical spectrum is in a good agreement with the Fourier prediction of 260 fs for the pulse duration.

Figure 7 shows typical RF spectra of a 9.87 MHz sub-picosecond pulse train, up to the highest order at 7 GHz. A spectral resolution less than 3 kHz of the spectrum analyzer enabled us to detect all noise components accurately which is necessary to evaluate energy fluctuations and timing jitter at different output ports (see inset of Fig. 8).

A mode-locked laser may generate pulses which are accompanied by various kinds of noises [14]. The RF spectrum of an optical pulse without any jitter consists of discrete modes with a frequency spacing of $n\omega_c$ where ω_c is the longitudinal mode spacing of the laser cavity and n is the mode number. Due to jitter, each harmonic consists of sum of a constant amplitude noise spectrum due to the pulse energy fluctuations and a component from pulse duration fluctuations and timing jitter. To obtain the phase and energy jitter, the simplified relations from von der Linde method is used [15]. Based on the definitions for the nth order frequency component, P_A, P_B, and P_D represent the absolute maximum powers of: signal spike, structure with frequency width of Δf_j and the broad noise band with a full width at half maximum of Δf_A (see inset Fig. 8). On the other hand, a detailed analysis in low-resolution spectra shows that the lowest noise bands represented by the ratios P_D/P_A are actually the sum of two different contributions: (i) middle narrow noise bands due to a fast temporal jitter with the power of P_c and a frequency width of $\Delta f'_j$ and (ii) constant broad noise bands (noise floor) due to amplitude fluctuations with a power level of P_D and a frequency width of Δf_A. In proposed system, the contribution from pulse width fluctuations can be neglected due to the soliton nature of the pulses generated and the results are summarized below.

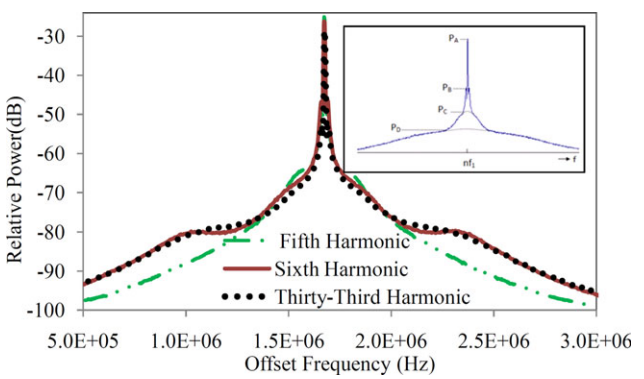

Figure 8 Typical spectra of different harmonics as a function of the scaled offset frequency for a sub-picosecond pulse train at output port of PBS. The RBW in RFSA is fixed at 3 kHz. Inset shows the noise structure and marks P_A, P_B, P_C, and P_D. [Color figure can be viewed in the online issue, which is available at wileyonlinelibrary.com]

Ratios of P_D/P_A, P_C/P_A, and P_B/P_A at the 10% coupler port, were found to be 6.2×10^{-6}, 1.7×10^{-3}, and 7.6×10^{-3}, respectively. However, for PBS port, the minimum values for P_D/P_A and P_C/P_A were measured to be 2.4×10^{-5} and 3.4×10^{-4}, respectively. Meanwhile, P_B/P_A remained constant. As a result, the pulse energy fluctuation at the coupler port is lower than the PBS port. It should be noted that, operating with a CW background, increased timing jitter up to 14 ps. For small timing-jitter, all the harmonics can be described by a Gaussian profile, whose widths increase proportional to the harmonic number. As the harmonic number increases, the tail's deviation increases as well. Note that the peak values of the different harmonics decay with a rate of $1/\omega$. The influence of longer time scale fluctuations on lower frequencies of the power spectrum modifies the shapes toward Lorentzians and makes their FWHM's smaller. This effect leads to higher-order dependence of the FWHM spectra on the harmonic number. It is found that when timing-jitter fluctuations between successive neighboring pulses are uncorrelated in time, different harmonics have Lorentzian shaped spectra. The FWHM for each harmonic in the spectrum is proportional to the square of the harmonic number. Effects of correlations between the timing fluctuations of neighboring pulses in the train, tend to produce spectra at different harmonics, which are both Gaussian in shape and have FWHM's that increase linearly with harmonic number.

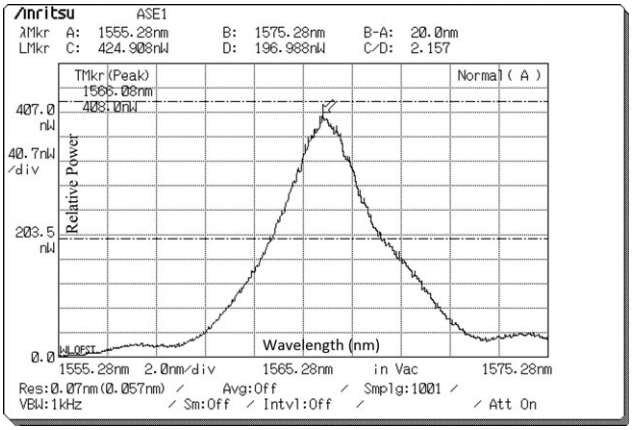

Figure 9 Spectrum measured at PBS port for an optimal setting

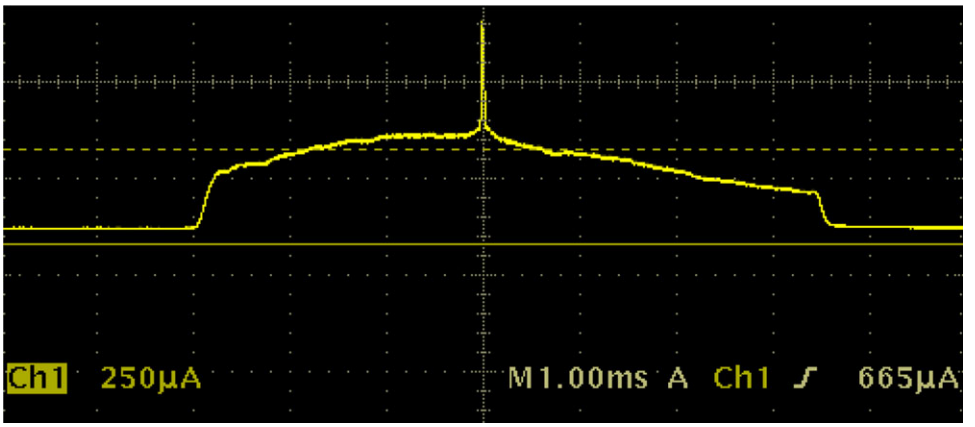

Figure 10 Autocorrelation trace and pulse train (inset) of the 130 ps pulses. [Color figure can be viewed in the online issue, which is available at wileyonlinelibrary.com]

A comparison of the energy fluctuations at the PBS port and the coupler port reveals that energy fluctuation from the coupler port to the PBS port is varied from 4.1% to 7.8%. For a fixed pump power of 92 mW, the low and high frequency jitter at the coupler port were measured to be 11.5 ps and 13.8 ps, correspondingly. Although, at PBS port, these values can reach up to 17.5 ps and 40 ps, respectively. Note that, the true noise of the laser may be lower, since amplitude-to-phase conversion in the photo detection process is already limited by the current measurements. A low cavity loss would result in low phase noise and timing jitters because of the reduction of spontaneous emission. Hence the lowest timing jitter and the lowest pulse amplitude noise were achieved by optimizing the cavity loss and simply by removing the used connectors (four) from the setup. In the absence of a feedback loop for controlling the pump power and a temperature-sealed box for laser cavity, the jitters are larger than the corresponding pulse durations. This is due to limitations imposed by soliton lasers where large nonlinearities result in relatively high timing jitter [18].

The measured low frequency jitter at the maximum pump power was about 4 ps at the coupler port while it can be reached up to 6 ps at PBS port. It was found that the energy fluctuations are related to bandwidth of optical spectrum such that a broader spectral bandwidth yields a smaller energy fluctuation in the system. The low frequency jitter noise is inversely proportional to the pump power such. By removing fiber adapters, controlling the environmental airflow in the setup, using a pump source with a fluctuation limit of less than 0.10% and a temperature controller with an accuracy of $\pm 0.01^{\circ}$C, timing jitter was reduced by an order of magnitude.

By decreasing the lengths of fibers (SMFs) with negative GVDs, the spectrum would be further narrowed and the nonlinear effects would become almost absent. Results show that the system with a high positive net GVD (ps^2) reaches mode locking fast. However the pulse width becomes broader because the SPM does not generate new frequencies in the leading edge and trailing edge of the spectrum. However, it is possible to increase the nonlinear coefficient of the fiber (γ) so that a broader spectrum could be obtained. It is worth noting that the nonlinear coefficient (γ) of SMF is much smaller than the γ for EDF in the setups. Alternatively, by cutting off a piece of SMF and placing it in a appropriate position, it is feasible to change the peak intensities and nonlinearities within the cavity without changing the net dispersion of the cavity.

A smaller dispersion to SPM ratio enabled us to achieve the pulses as short as 131 fs. The measured FWHM of 20 nm in Figure 9 is in a good agreement with the Fourier prediction of 130 fs pulses (see Fig. 10).

By increasing pump power and optimizing the output coupling ratios, one can further reduce the time-bandwidth products (TBWP), pulse duration, and output fluctuations [15].

6. CONCLUSION

We have demonstrated a near transform limited passively mode locked laser in which the pulse width can be continuously tuned from 1.2 ps up to less than 131 fs with a maximum spectral width of 20 nm. A smaller dispersion to SPM ratio enabled us to achieve pulses with energy fluctuations of less than 2.5%. A comparison of the energy fluctuations at PBS port and coupler port reveals that energy fluctuation from coupler port to PBS port is varied from 4.1% to 7.8%. The low and high frequency jitter at coupler port for a fixed pump power of 92 mW were measured to be 11.5 ps and 13.8 ps respectively. Although, it can be reached up to 17.5 ps and 40 ps at PBS port. By removing fiber adapters and controlling the environmental airflow in the setup, timing jitter was reduced by an order of magnitude.

REFERENCES

1. H. Abramczyk, Introduction to laser spectroscopy, Elsevier Science, 2005.
2. U. Keller, D. Miller, G. Boyd, T. Chiu, J. Ferguson, and M. Asom, Opt Lett 17 (1992), 505–507.
3. C. Hönninger, M. Plötner, B. Ortaç, R. Ackermann, R. Kammel, J. Limpert, S. Nolte, and A. Tünnermann, Femtosecond fiber laser system for medical applications, in, 2009, pp. 72030W.
4. T. Kiatchanog, K. Igarashi, T. Tanemura, D. Wang, K. Katoh, and K. Kikuchi, Real-time all-optical waveform sampling using a passively mode-locked fiber laser as the sampling pulse source, In Optical Fiber Communication Conference(OFC), IEEE, Anaheim, CA, 2006, p. 3.
5. M. Attygalle, C. Lim, and A. Nirmalathas, Dispersion-tolerant multiple WDM channel millimeter-wave signal generation using a single monolithic mode-locked semiconductor laser, J Lightwave Technol 23 (2005), 295.
6. T. Mizunami and A. Ehara, Femtosecond-pulsed laser micromachining and optical damage by an erbium-doped fiber-laser system, Microelectron Eng 88 (2011) 2334–2337.
7. U. Kellers, Laser physics and applications, Springer-Verlag, Berlin, 2007, subvolume B, part 1.
8. E. Ippen, Ultrafast dynamics of quantum systems physical processes and spectroscopic techniques, Baldassare Di Bartolo and Giulio

Gambarota, Femtosecond Pulse Generation: Principles and Fiber Applications, (2002), 213–231.
9. M. Nakazawa, E. Yoshida, Y. Kimura, Generation of 98 fs optical pulses directly from an erbium-doped fibre ring laser at 1.57 μm, Electron Lett 29, (1993), 63.
10. U. Keller, K.J. Weingarten, F.X. Kartner, D. Kopf, B. Braun, I.D. Jung, R. Fluck, C. Honninger, N. Matuschek, and J. Aus der Au, Semiconductor saturable absorber mirrors (SESAM's) for femtosecond to nanosecond pulse generation in solid-state lasers, Select Top Quant Electron IEEE J 2 (1996), 435–453.
11. I. Walmsley, L. Waxer, and C. Dorrer, The role of dispersion in ultrafast optics, Rev Sci Instrum 72 (2001), 1.
12. R. Paschotta, Encyclopedia of laser physics and technology, Wiley-VCH, 2008.
13. H. Zhang, Arxiv preprint arXiv:1111.4502, (2011).
14. C.X. Yu, Noise characteristics of the fiber ring lasers, in: Department of Electrical Engineering and Computer Science Massachusetts Institute of Technology, Cambridge, MA, 1996.
15. M.R.A. Moghaddam, S. Harun, R. Akbari, and H. Ahmad, Laser Phys 21 (2011), 1–6.

A FULLY INTEGRATED 40-Gb/s CDR WITH EIGHT-PHASE VCO FOR OPTICAL FIBER COMMUNICATION*

Yingmei Chen, Shuangchao Yan, Zhigong Wang, Li Zhang, and Wei Li
Institute of RF- & OE-ICs, Southeast University, 210096 Nanjing, China; Corresponding author: njcym@seu.edu.cn

Received 23 April 2012

ABSTRACT: *This article presents a fully integrated 40-Gb/s phase locked clock and data recovery (CDR) circuit with 1:4 demultiplexer (DEMUX) in International Business Machines (IBM) 90-nm CMOS technology. The CDR circuit incorporates a novel eight-phase CL ladder filtering voltage-controlled oscillator and a quarter rate bang-bang phase detector. The 40-Gb/s input data are sampled with eight parallel differential master-salve flip-flops every 12.5 ps and the 40-Gb/s data are demultiplexed into four 10-Gb/s outputs when the CDR circuit is phase locked. The recovered and frequency divided 10-GHz clock has a phase noise of −101.01 dBc/Hz at 1 MHz offset and a peak to peak jitter of 3.4 ps. The CDR and 1:4 DEMUX consumes 72 mW from a 1.2 V supply excluding out buffers.* © 2012 Wiley Periodicals, Inc.
Microwave Opt Technol Lett 55:170–173, 2013; View this article online at wileyonlinelibrary.com. DOI 10.1002/mop.27248

Key words: *CDR; demultiplexer; phase detector; voltage controlled oscillator; CL ladder filter*

1. INTRODUCTION

Clock and data recovery (CDR) circuits operating at tens of gigabits per second in optical communication system pose difficult challenges with respects to device, speed, jitter, signal distribution, system architecture, and power consumption. The first 40-Gb/s CDR circuit with quarter rate architecture in 0.18-μm CMOS technology was presented in 2003 [1], but it produces a large clock jitter of 0.9 ps_{rms} and 9.67 ps_{pp}, and a large chip area. Full-rate 40-Gb/s CDR circuits have been implemented in 90-nm CMOS technology [2] and bipolar technology [3, 4], but it has a large retimed data jitter of 9.6 ps_{pp} in Ref. 2, and they require 5-V supply and draw 1.6–5 W in Refs.3 and 4. The design of low phase noise, less inductor, and low phase error eight-phase voltage-controlled oscillator (VCO) and design of phase detector (PD) capable of operating at 40-Gb/s become increasing more difficult as the supply voltage scales down. It is important to do further research on novel circuit topologies and new system architecture to meet the requirement of higher speed, low voltage, and low power.

The focus in this article is to demonstrate a 40-Gb/s CDR circuit designed in IBM 90-nm CMOS technology. Base on a quarter rate topology, the architecture includes an inductor-less eight-phase LC oscillator and a quarter-rate bang-bang PD functioning data retiming and 1:4 demultiplexer (DEMUX) [5]. The CDR circuit eliminates the need of 1:4 DEMUX block, thereby achieving low power consumption and small chip area. The architecture and design issues of the quarter rate CDR are described in Section 2, and Section 3 deals with the design of the building blocks. Section 4 summarizes the post simulation results.

Project supported by the National Natural Science Foundation of China (No. 60976029) and the National High Technology Research and Development Program of China (No. 2011AA010301).

2. CDR ARCHITECTURE

With a data of 40-Gb/s in 90-nm CMOS process, many design issues at the circuit and the architecture levels must be considered. The CDR circuit uses a quarter rate architecture to relax the technology-related difficulties, such as limited device speed and low supply voltage. As shown in Figure 1, the CDR architecture consists of a VCO, a PD, voltage–current (V/I) converters, a low-pass filter, and the system works as follows.

At the startup, the 10-GHz clocks provided by eight-phase VCO with 45° phase difference every two consecutive clock sample the input 40-Gb/s data every 12.5 ps and then produce eight samples in one clock period. The quarter rate PD processes these samples and produce early/late signals to V/I converter which will charge into or out of the loop filter according to the early/late signal. The low-pass filter provides the clock information extracted from the charge or discharge current to VCO. When the CDR circuit is locked, four of the eight clocks will align to the middle of the data, retiming and demultiplexing the 40-Gb/s input into four 10-Gb/s outputs. In the absence of data transition, the V/I converter generates no output current, leaving the VCO control line undisturbed.

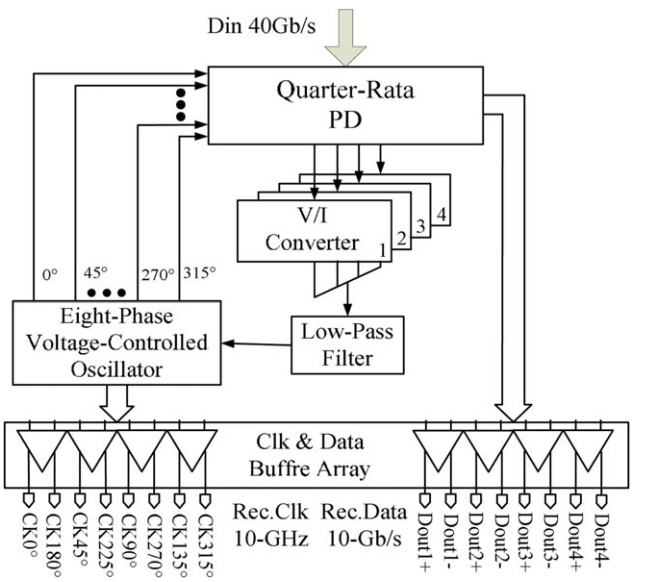

Figure 1 CDR architecture